INTERNATIONAL JOURNAL FOR NUMERICAL METHODS IN FLUIDS, VOL. 16, 597–612 (1993)

INCOMPRESSIBLE LOW-SPEED-RATIO FLOW IN NON-UNIFORM DISTENSIBLE TUBES*

P. J. REUDERINK, F. N. VAN DE VOSSE, A. A. VAN STEENHOVEN, M. E. H. VAN DONGEN† AND J. D. JANSSEN

Departments of Mechanical Engineering and Physics†, Eindhoven University of Technology, P.O. Box 513, 5600 MB Eindhoven, The Netherlands

SUMMARY

The fluid flow in distensible tubes is analysed by a finite element method based on an uncoupled solution of the equations of wall motion and fluid flow. Special attention is paid to the choice of proper boundary conditions. Computations were made for sinusoidal flow in a distensible uniform tube with the Womersley parameter $\alpha = 5$, and a ratio between tube radius and wavelength from 0·0001 to 0·5. The agreement between the numerical results and Womersley's analytic solution depends on the speed ratio between fluid and wave velocity, and is fair for speed ratios up to 0·05. The analysis of the flow field in a distensible tube with a local inhomogeneity revealed a marked influence of wave phenomena and wall motion on the velocity profiles.

KEY WORDS Navier–Stokes equations Finite element method Distensible tubes Wave propagation

INTRODUCTION

In the analysis of the flow phenomena in distensible geometries, as found, for example, in arteries, not only the equations of fluid flow but also the equations governing wall motion must be taken into account. In many cases it is impracticable to obtain a coupled numerical solution of the equations of fluid flow and wall motion. The distinct ways in which the motion of the fluid and the wall are described, the inconvenient shape of the set of discretized equations, and the large amount of CPU time required to solve this coupled set of equations play a role in this respect. An alternative is the 'weakly coupled' solution of the fluid and wall motion equations. In this approach the equations of fluid flow are solved for a specific time step with appropriate boundary conditions describing the position and movement of the wall at this time step. From the solution for the fluid flow the forces acting on the wall can be computed. In principle, it should be possible to compute the position and movement of the wall at the next time step from these forces using an appropriate extrapolation algorithm. Hilbert[1] applied such a strategy to compute the fluid flow in a uniform distensible tube. Even though Hilbert made calculations for a tube in which accelerations of the wall were reduced considerably by taking a large mass of this wall per unit area, he experienced numerical convergence and stability problems common to this type of strategy, and an appropriate extrapolation algorithm could only be found empirically.

To circumvent these problems, Reuderink *et al.*[2] proposed a numerical approach for an uncoupled solution of the equations of wall motion and the equations of fluid flow. The feature of

* This research project is supported by the Dutch Foundation for Scientific Research NWO.

0271–2091/93/070597–16$13.00

Received August 1992
Revised November 1992

this approach is the assumption that the wall motion can be calculated on the basis of the pressures due to wave phenomena. Motion of the wall is caused by changes in pressure and wall shear stress. The latter will be neglected in this study since they have only a minor influence on the longitudinal wall motion in the cases of interest to us. The pressure in a distensible geometry is the result of wave phenomena and local fluid effects. The wave phenomena are a direct consequence of the interaction between the fluid and the distensible wall. Pressure and flow disturbances travel through the system with a finite wave velocity. The pressures corresponding to this wave phenomena have a magnitude $\mathcal{O}(\rho cu)$, with ρ the density of the fluid, c the wave velocity and u the fluid velocity (Reference 3). Changes in pressure due to local fluid effects, like convective effects associated with the curvature of the vessel, have a magnitude $\mathcal{O}(\frac{1}{2}\rho u^2)$. This yields that the pressure is mainly dependent on wave phenomena if the ratio between fluid and wave velocity, which we will refer to as the speed ratio S, is much smaller than unity. This holds in a number of situations, for example, for the flow in arteries, where usually $S<0{\cdot}1$ (see Reference 4). Therefore, the first step in our approach is the calculation of the time-dependent pressure distribution due to wave phenomena. Next, the wall motion due to this time-dependent pressure distribution is calculated. Finally, this wall motion is prescribed as a boundary condition for the equations for the fluid flow.

In this paper, first a more detailed outline of this approach will be given. Next, the results of calculations for a uniform distensible tube will be presented. For this case an analytical solution is described by Womersley,[5] enabling us to evaluate several aspects of the numerical method used to solve the fluid equations. Finally, the numerical approach is used to calculate the velocity field in a uniform elastic tube with a local inhomogeneity.

OUTLINE OF THE METHOD

Our approach for the numerical analysis of the flow phenomena in distensible geometries is based on an uncoupled solution of fluid and wall motion equations, following three steps:

1. The time-dependent pressure distribution is calculated using a quasi-one-dimensional model describing the propagation of pressure waves generated at the entrance of the distensible geometry. The assumption of one-dimensionality holds if the tube radius is much smaller than the wavelength, which is the case, for example, for wave propagation in arteries (see Reference 4). In this study we use a linear model assuming that the fluid velocity is much smaller than the wave velocity. This one-dimensional (1D) linear model is verified experimentally for uniform, reflectionless, latex tubes[6,7] and can be extended to incorporate reflection phenomena as occurring, for example, in the carotid artery bifurcation.[8] As an input for this wave propagation model, the dynamic pressure-area relations at various locations in the geometry are needed, which are usually determined experimentally.
2. From the time-dependent pressure distribution, the wall motion can be calculated. In general, this will require the development of a numerical model on the basis of geometrically non-linear deformation theory and an appropriate material model. However, for the situations discussed in this study, the wall motion is calculated analytically from the pressure distribution and the experimentally determined pressure–area relations already mentioned above.
3. The fluid flow is described by the Navier–Stokes equation, which can be solved numerically. The numerical method used for this purpose is described in more detail in the next section. Apart from the appropriate time-dependent inflow and outflow conditions, the position of the wall is updated and the correct fluid velocity at the wall is prescribed as a boundary

condition using the results of the calculations of the wall motion mentioned in the previous step.

GENERAL FLUID FLOW

The flow of an incompressible isothermal Newtonian fluid is described by the Navier–Stokes equation and continuity equation. To solve these equations, a spatial discretization is applied using Galerkin's finite element method. This results in the following set of non-linear first-order differential equations (see, for instance, References 9–11):

$$\mathbf{M}\dot{\mathbf{u}} + [\mathbf{S} + \mathbf{N}(\mathbf{u})]\mathbf{u} + \mathbf{L}^{\mathrm{T}}\mathbf{p} = \mathbf{f} + \mathbf{b}, \tag{1}$$

$$\mathbf{L}\mathbf{u} = \mathbf{0}, \tag{2}$$

where $\mathbf{M}\dot{\mathbf{u}}$ represents the local acceleration term, $\mathbf{S}\mathbf{u}$ the viscous term, $\mathbf{N}(\mathbf{u})\mathbf{u}$ the convective acceleration term, $\mathbf{L}^{\mathrm{T}}\mathbf{p}$ the pressure gradient term, and $\mathbf{L}\mathbf{u}$ the velocity divergence term. On the right-hand side, $\mathbf{f}$ and $\mathbf{b}$ represent the body and boundary forces, respectively. Finally, the columns $\mathbf{u}$ and $\mathbf{p}$ contain the velocity and pressure unknowns in the interpolation points, respectively. The element used is the modified Crouzeix–Raviart element, with 1 pressure and 2 pressure-gradient unknowns and 14 velocity unknowns for 2D calculations. The accuracy is $\mathcal{O}(h^3)$ for the velocity and $\mathcal{O}(h^2)$ for the pressure, h being a characteristic dimension of the finite element in the mesh. To avoid partial pivoting, the set of equations (1) and (2) was uncoupled with a penalty-function method. To this end, the discretized continuity equation (2) is replaced by

$$\mathbf{L}\mathbf{u} = \varepsilon \mathbf{M}_{\mathrm{p}}\mathbf{p}, \tag{3}$$

where the penalty-function parameter ε is chosen to be sufficiently small in order to comply with the incompressibility of the fluid. When the time derivative in the discretized momentum equation (1) is approximated by a finite difference method, this equation can be rewritten[13] as

$$\mathbf{M}\frac{\mathbf{u}^{n+1}-\mathbf{u}^{n}}{\Delta t} + \left[\mathbf{S} + \mathbf{N}(\mathbf{u}^{n+\theta}) + \frac{1}{\varepsilon}\mathbf{L}^{\mathrm{T}}\mathbf{M}_{\mathrm{p}}^{-1}\mathbf{L}\right]\mathbf{u}^{n+\theta} = \mathbf{f}^{n+\theta} + \mathbf{b}^{n+\theta}, \tag{4}$$

$$\mathbf{p}^{n+1} = \frac{1}{\varepsilon}\mathbf{M}_{\mathrm{p}}^{-1}\mathbf{L}\mathbf{u}^{n+1}. \tag{5}$$

Here n denotes the time-step number. For $\theta = 1$ this scheme reduces to the Euler-implicit scheme having an accuracy of $\mathcal{O}(\Delta t)$ for linear equations, while for $\theta = \frac{1}{2}$ this scheme reduces to a Crank–Nicolson-type method which is $\mathcal{O}(\Delta t^2)$ accurate for linear equations. The non-linear convective term $\mathbf{N}(\mathbf{u}^{n+\theta})\mathbf{u}^{n+\theta}$ is linearized using one step of a Newton–Raphson iteration scheme

$$\mathbf{N}(\mathbf{u}^{n+\theta})\mathbf{u}^{n+\theta} = \mathbf{J}(\mathbf{u}^{n})\mathbf{u}^{n+\theta} - \mathbf{N}(\mathbf{u}^{n})\mathbf{u}^{n}, \tag{6}$$

where $\mathbf{J}$ is the Jacobian matrix of $\mathbf{N}$. Together with the equation

$$\mathbf{u}^{n+\theta} = \theta\mathbf{u}^{n+1} + (1-\theta)\mathbf{u}^{n}, \tag{7}$$

this linearization technique results in

$$\left[\frac{\mathbf{M}}{\theta\Delta t} + \mathbf{S} + \mathbf{J}(\mathbf{u}^{n}) + \frac{1}{\varepsilon}\mathbf{L}^{\mathrm{T}}\mathbf{M}_{\mathrm{p}}^{-1}\mathbf{L}\right]\mathbf{u}^{n+\theta} = \left[\frac{\mathbf{M}}{\theta\Delta t} + \mathbf{N}(\mathbf{u}^{n})\right]\mathbf{u}^{n} + \mathbf{f}^{n+\theta} + \mathbf{b}^{n+\theta}. \tag{8}$$

This equation shows how, starting with a solution $\mathbf{u}^{n}$ at time step n, the solution $\mathbf{u}^{n+\theta}$ is calculated for time step $n+\theta$ using an Euler-implicit step. Next, the solution $\mathbf{u}^{n+1}$ can be calculated by extrapolation from $\mathbf{u}^{n+\theta}$ and $\mathbf{u}^{n}$ using equation (7).

FLOW IN A DISTENSIBLE UNIFORM TUBE

Governing equations

The flow field in a uniform distensible tube with radius R and a length equal to 2 times the wavelength λ, filled with a Newtonian fluid with density ρ and dynamic viscosity η will be analysed. Due to its cylindrical symmetry, the problem is two-dimensional. For a description of the flow in this tube it is convenient to introduce the following dimensionless quantities:

$$r'=\frac{r}{R},\quad z'=\frac{z}{\lambda},\quad u'=\frac{u\lambda}{|\bar{w}|R},\quad w'=\frac{w}{|\bar{w}|},\quad t'=\frac{tc_1}{\lambda},\quad p'=\frac{p}{\rho c_1|\bar{w}|},\quad \sigma'=\frac{\sigma}{\rho c_1|\bar{w}|}, \tag{9}$$

with r and z the radial and axial co-ordinates, respectively, u and w the radial and axial velocity components, respectively, $|w|$ the amplitude of the cross-sectionally averaged axial velocity, c_1 the wave velocity, and σ the stress tensor. If no reflections are present in the tube, the time-dependent pressure distribution is described using the linear quasi-1D model by a travelling wave:

$$p(z,t)=\mathrm{Re}\,[p_0 e^{jw(t-z/c)}], \tag{10}$$

where p_0 is a complex number describing the amplitude and phase of the pressure at the entrance $z=0$ at time $t=0$ and Re[·] denotes the real part of [·]. For convenience, we will take the phase of p_0 equal to zero, so that p_0 is the same as the pressure amplitude at the entrance $z=0$. The complex wave velocity is represented by c, of which the real part describes the wave velocity c_1, while the imaginary part describes the damping of the wave. For a tube under 'maximal longitudinal constraint', an assumption usually made for arteries, meaning that no longitudinal wall motion is possible, the complex wave velocity c is given by the linear quasi-1D model as[6,7]

$$c=\left\{\frac{\pi R^2}{\rho C}[1-F_{10}(\alpha)]\right\}^{1/2}, \tag{11}$$

where C is the compliance of the tube, which is a measure for the ratio between pressure and cross-sectional area changes, and F_{10} is a function of Womersley's parameter $\alpha=R\sqrt{(\omega\rho/\eta)}$. Instead of choosing a value for the compliance C for our test situation, from which the complex wave speed can be computed, we directly chose a value for the wave velocity c_1. For elastic wall behaviour, there is no phase difference between pressure and cross-sectional area oscillations and the compliance C is real. Therefore, the imaginary part of the complex wave velocity corresponding to our choice of the wave velocity c_1 can be calculated using equation (11) as

$$\frac{\mathrm{Im}[c]}{c_1}=\frac{\mathrm{Im}\,[(1-F_{10}(\alpha))^{1/2}]}{\mathrm{Re}\,[(1-F_{10}(\alpha))^{1/2}]}. \tag{12}$$

Using equations (9) and (12), dropping the accents, equation (10) can be rewritten in a dimensionless form as

$$p(z,t)=\mathrm{Re}\,[p_0 e^{2\pi j(t-z\psi^{-1}(\alpha))}], \tag{13}$$

where $\psi(\alpha)$ is defined as $\psi(\alpha)=c/c_1$.

As a next step, the wall motion is calculated based on linear deformation theory, which yields, for a tube under maximal longitudinal constraint,

$$\zeta(z,t)=0, \tag{14}$$

$$\xi(z,t)=\mathrm{Re}\left\{\frac{p_0}{2}S\psi(\alpha)^2[1-F_{10}(\alpha)]\,e^{2\pi j[t-z\psi^{-1}(\alpha)]}\right\}, \tag{15}$$

where ζ and ξ represent the longitudinal and radial wall motion, respectively. Please note that equation (15) indicates that the relative diameter change at a given value of Womersley's parameter α is directly proportional to the speed ratio $S=|\bar{w}|/c_1$.

The r and z components of the Navier–Stokes equation and the continuity equation, written in dimensionless form using equations (9), yield

$$\frac{\partial u}{\partial t}+\alpha^{-2}\left\{\frac{\partial}{\partial r}\left[\frac{1}{r}\frac{\partial}{\partial r}(ur)\right]+G^2\frac{\partial^2 u}{\partial z^2}\right\}+S\left(u\frac{\partial u}{\partial r}+w\frac{\partial u}{\partial z}\right)=-\frac{1}{G^2}\frac{\partial p}{\partial r}, \tag{16}$$

$$\frac{\partial w}{\partial t}+\alpha^{-2}\left[\frac{1}{r}\frac{\partial}{\partial r}\left(r\frac{\partial w}{\partial r}\right)+G^2\frac{\partial^2 w}{\partial z^2}\right]+S\left(u\frac{\partial w}{\partial r}+w\frac{\partial w}{\partial z}\right)=-\frac{\partial p}{\partial r}, \tag{17}$$

$$\frac{1}{r}\frac{\partial}{\partial r}(ur)+\frac{\partial w}{\partial z}=0, \tag{18}$$

where $G=R/\lambda$ is the ratio between tube radius and wavelength. From the preceding equations, it is clear that the flow problem can be characterized by three dimensionless numbers: α, S and G. An analytic coupled solution of the wall motion and fluid flow is given by Womersley[5] for situations where $S\ll 1$ and $G\ll 1$.

Spatial discretization

The element mesh used for the calculations is shown in Figure 1. The geometry of the tube changes as described by equations (14) and (15) due to the motion of the wall. The figure shows the shape at $t=0$. The length of the tube is chosen equal to two wavelengths. The mesh can be mapped on a rectangular grid and contains eight elements in the radial direction and 64 in the axial direction. Because the geometry of the tube changes, the mesh is updated for each time step; this is done without changing its topology. Since the displacements per time step are small, the solution $\mathbf{u}^n$ calculated for the nodal points of the old mesh could serve as a starting solution on the nodal points of the new mesh [see equation (8)].

Boundary conditions

Apart from the geometry, the boundary conditions are also time dependent. As inflow condition ($z=0$), the fully developed velocity profile, as calculated by Womersley,[5] is prescribed in a dimensionless form given by

$$w(r, z, t)=\mathrm{Re}\left\{p_0\psi(\alpha)\left[1-\frac{J_0(\alpha j^{3/2}r)}{J_0(\alpha j^{3/2})}\right]e^{2\pi j(t-z\psi^{-1}(\alpha))}\right\}, \tag{19}$$

$$u(r, z, t)=\mathrm{Re}\left\{\pi j p_0 S\psi^2(\alpha)\left[\frac{2J_1(\alpha j^{3/2}r)}{\alpha j^{3/2}J_0(\alpha j^{3/2})}+r\right]e^{2\pi j(t-z\psi^{-1}(\alpha))}\right\}. \tag{20}$$

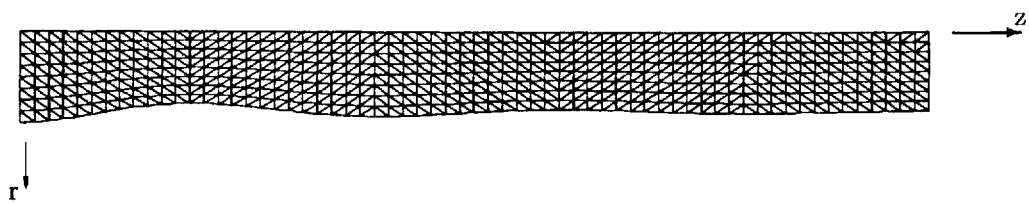

Figure 1. The element mesh used for the uniform distensible tube

The boundary conditions at the tube axis are based on symmetry considerations:

$$\left.\frac{\partial w}{\partial r}\right|_{r=0}=0, \qquad \left.u\right|_{r=0}=0, \tag{21}$$

while the boundary conditions of the wall are obtained by taking the time derivatives of the wall displacements:

$$\left.w\right|_{r=R}=\frac{\partial \zeta}{\partial t}, \qquad \left.u\right|_{r=R}=\frac{\partial \xi}{\partial t}. \tag{22}$$

There are several possibilities for the outflow conditions:

1. The radial and axial velocity profiles, u and w, as described by equations (19) and (20), respectively, are prescribed.
2. The normal and tangential components of the stress vector, σ_n and σ_t, which, in axisymmetric cylinder co-ordinates, are given, respectively, by

$$\sigma_n=\frac{4\pi G^2}{\alpha^2}\frac{\partial w}{\partial z}-p, \tag{23}$$

$$\sigma_t=\frac{4\pi G^2}{\alpha^2}\left(\frac{\partial w}{\partial r}+\frac{\partial u}{\partial z}\right), \tag{24}$$

   can be prescribed by substitution of equations (19) and (20) in equations (23) and (24).
3. In general, knowledge about the velocity profiles as given by equations (19) and (20) is not available, and boundary conditions of type 1 or 2 cannot be applied. In that case one might use approximations for the stress components assuming that the contributions of the velocity gradients are negligible:

$$\sigma_n=-p, \tag{25}$$

$$\sigma_t=0. \tag{26}$$

Time integration and penalty-function parameter

For all calculations, the time integration was carried out over three successive flow cycles. Sixty four time steps were taken per flow cycle, when 128 time steps were taken, the solution was only $\mathcal{O}(10^{-5})$ different. For the first cycle, an Euler-implicit time integration scheme ($\theta=1$) was chosen to damp out errors induced by the initial condition.[13] For the two subsequent cycles, a Crank–Nicolson scheme ($\theta=\frac{1}{2}$) was taken to obtain a higher-order accuracy. After completion of the third flow cycle, the time integration was finished, because the solution obtained by carrying out an additional flow cycle showed a difference of $\mathcal{O}(10^{-5})$.

The penalty-function parameter was taken equal to $\varepsilon=10^{-6}$ for all calculations, except the ones with $G=0{\cdot}5$ and $G=0{\cdot}1$. Here the penalty-function parameter had to be chosen equal to $\varepsilon=10^{-4}$ and $\varepsilon=5\times10^{-3}$, respectively, in order to obtain an accurate solution for the pressure distribution in the tube. In these cases the solutions obtained for the velocity were not significantly different from the solutions calculated with the penalty-function parameter equal to $\varepsilon=10^{-6}$.

Results and discussion

Table I gives an overview of the computations of the flow field in the distensible, uniform tube described by the equations given above. First, a calculation was carried out for very small fluid/wave velocity and radius/wavelength ratios, $S=0{\cdot}0005$ and $G=0{\cdot}001$. For these small values

Table I. An overview of the numerical calculations made for the uniform tube

α	S	G	Boundary condition	ε	Equation
5	0·0005	0·0001	type 2	10^{-6}	Navier–Stokes
5	0·05	0·0001	type 2	10^{-6}	Navier–Stokes
5	0·2	0·0001	type 2	10^{-6}	Navier–Stokes
5	0·2	0·0001	type 2*	10^{-6}	Navier–Stokes
5	0·0005	0·1	type 2	10^{-4}	Navier–Stokes
5	0·0005	0·5	type 2	5×10^{-3}	Navier–Stokes
5	0·2	0·0001	type 1	10^{-6}	Navier–Stokes
5	0·2	0·0001	type 3	10^{-6}	Navier–Stokes
5	0·2	0·0001	type 2	10^{-6}	Stokes

* Corrected inflow conditions; see text.

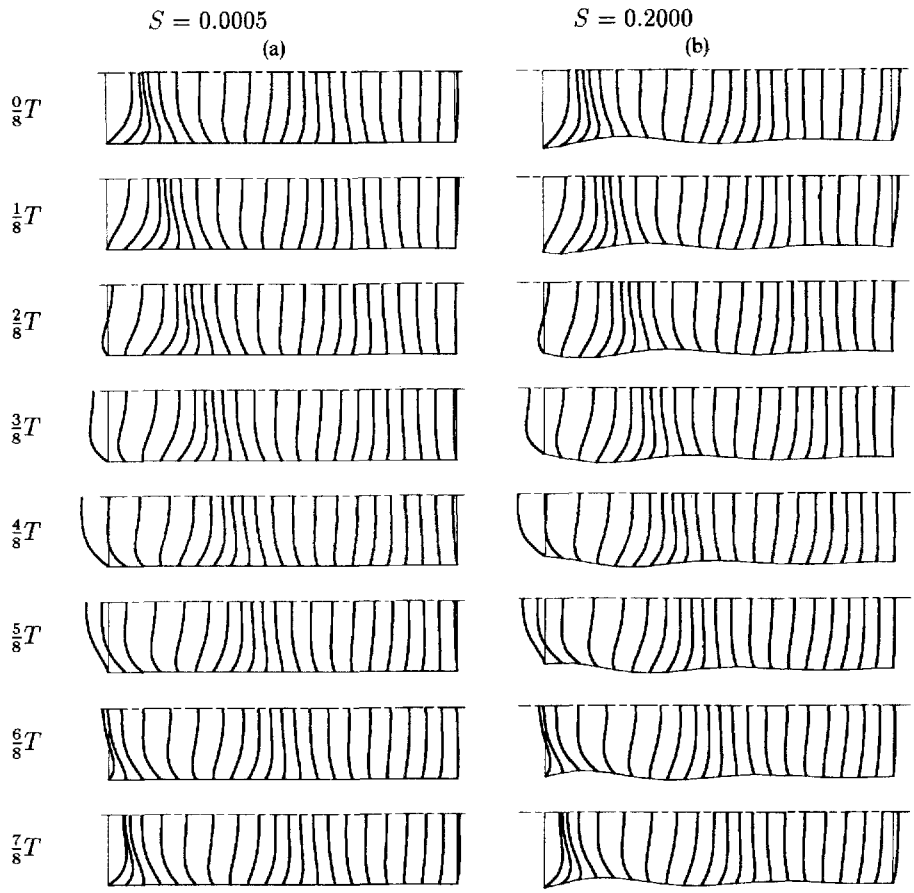

Figure 2. Axial velocity profiles at equidistant time steps for (a) $S=0{\cdot}0005$ and (b) $S=0{\cdot}2$, both with $G=0{\cdot}0001$. The dashed line represents the centre line of the tube. The inflow of the tube is at the left side

of S and G, Womersley's analytic solution should be valid. For this and all other cases discussed below, Womersley's parameter was chosen to be $\alpha=5$. Figure 2(a) shows the numerically predicted axial velocity profiles at various equidistant time steps. For this small speed ratio, the relative diameter change is only 0·01per cent [see equation (23)]. The propagation and damping

of the wave to the right part of the tube is clearly visible. Next, the influence of the magnitude of the speed ratio was analysed by increasing its value to $S=0{\cdot}05$ and $S=0{\cdot}2$, respectively. The results for $S=0{\cdot}2$ are shown in Figure 2(b). With the increase of the speed ratio, the relative diameter change increases to 10 per cent. Again the propagation of the wave to the right part of the tube is clearly visible. A remarkable difference with the results for $S=0{\cdot}0005$, as presented in Figure 2(a), is the presence of a net outflow at the distal end of the tube over a flow cycle. This is due to a non-linear effect of the fluid flow. As inflow condition, a velocity profile [equations (19) and (20)] corresponding to Womersley's analytical solution is prescribed in which the variation in cross-sectional area is neglected. This is not valid at large values of the speed ratio. The tube has a maximum entrance diameter during the phase of positive entrance flow, and a minimum entrance diameter during the phase of negative entrance flow. This results in a net inflow at the entrance over a flow cycle and a net outflow at the distal end.

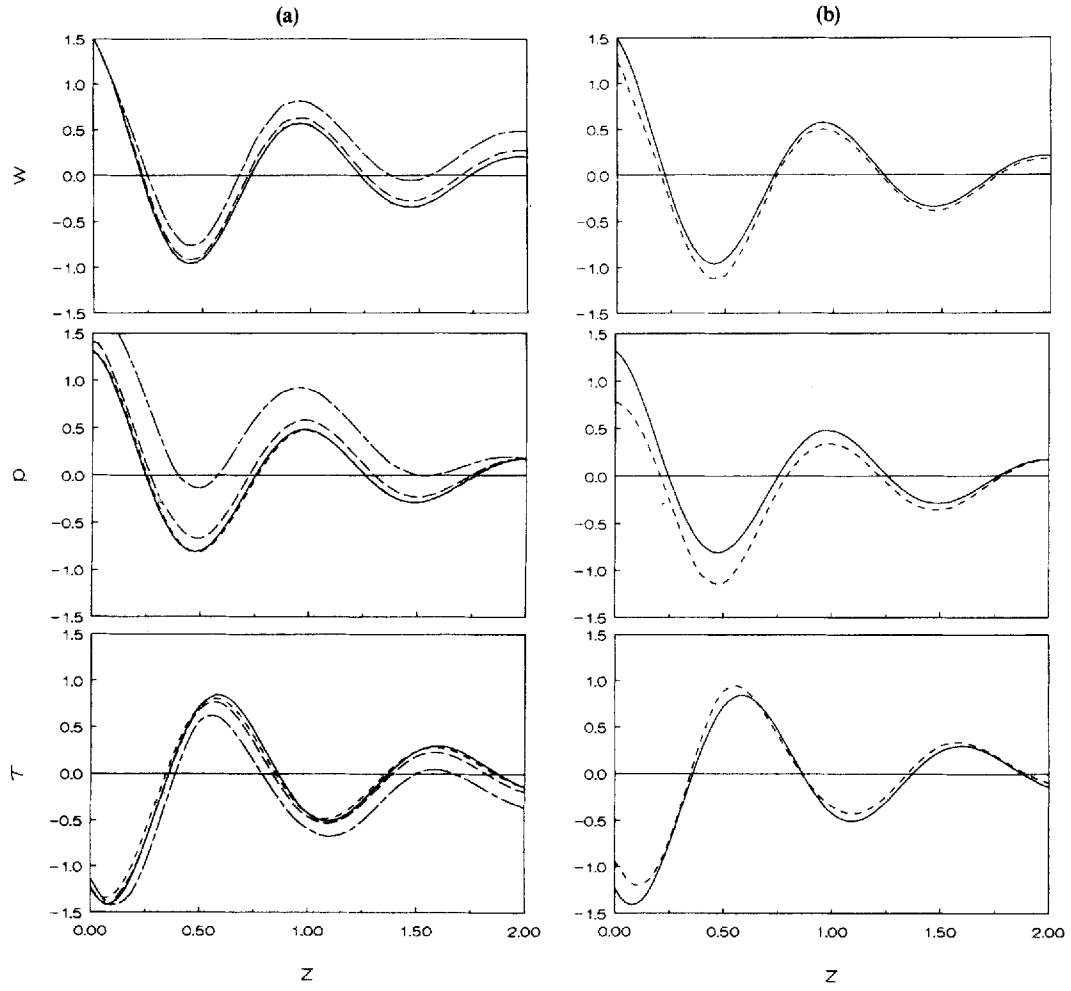

Figure 3. (a) Comparison of the axial velocity w on the tube axis (top panel), the pressure p on the tube axis (centre panel), and the wall shear stress τ_w (bottom panel) for values of $S=5\times10^{-4}$ (- - - -), $S=0{\cdot}05$ (— —) and $S=0{\cdot}2$ (— — — —) with the analytical results calculated using Womersley's theory (———). The results presented correspond to the solution at $t=0$.
(b) Same but only for $S=0{\cdot}2$ (- - - -) with a corrected flow inflow condition

In order to study the influence of the speed ratio in more detail, the computed axial velocity component and the pressure, both taken at the tube axis as a function of axial position, and the wall shear stress, as a function of axial position, are compared with the analytical solution obtained using Womersley's theory (Figure 3). The same is done for the profiles of the axial and radial velocity components taken along the tube radius at axial position $z = 1{\cdot}0$ (Figure 4). Except for the radial velocity component, a discrepancy is seen to increase with the value of the speed ratio, partly caused by the fact that there is a net inflow at the entrance. A sinusoidal flow at the entrance can be guaranteed by modifying the inflow conditions by multiplying the equation for the axial velocity component [equation (19)] by the time-dependent ratio of reference cross-sectional area and actual cross-sectional area. Figure 3(b) shows the results for this type of inflow condition at $S = 0{\cdot}2$. It is seen clearly that the magnitude of the discrepancies decreases towards the distal end of the tube, where the pressure oscillations and the resulting diameter changes are much smaller due to damping.

The influence of the magnitude of the ratio between radius and wavelength was analysed in the same way as was done for the speed ratio. Calculations were carried out for $G = 0{\cdot}1$ and $G = 0{\cdot}5$, both with $S = 0{\cdot}0005$ and $\alpha = 5$. Significant discrepancies between the analytical and the numerical solutions were found only for $G = 0{\cdot}5$. Relatively large values for G can be chosen without these

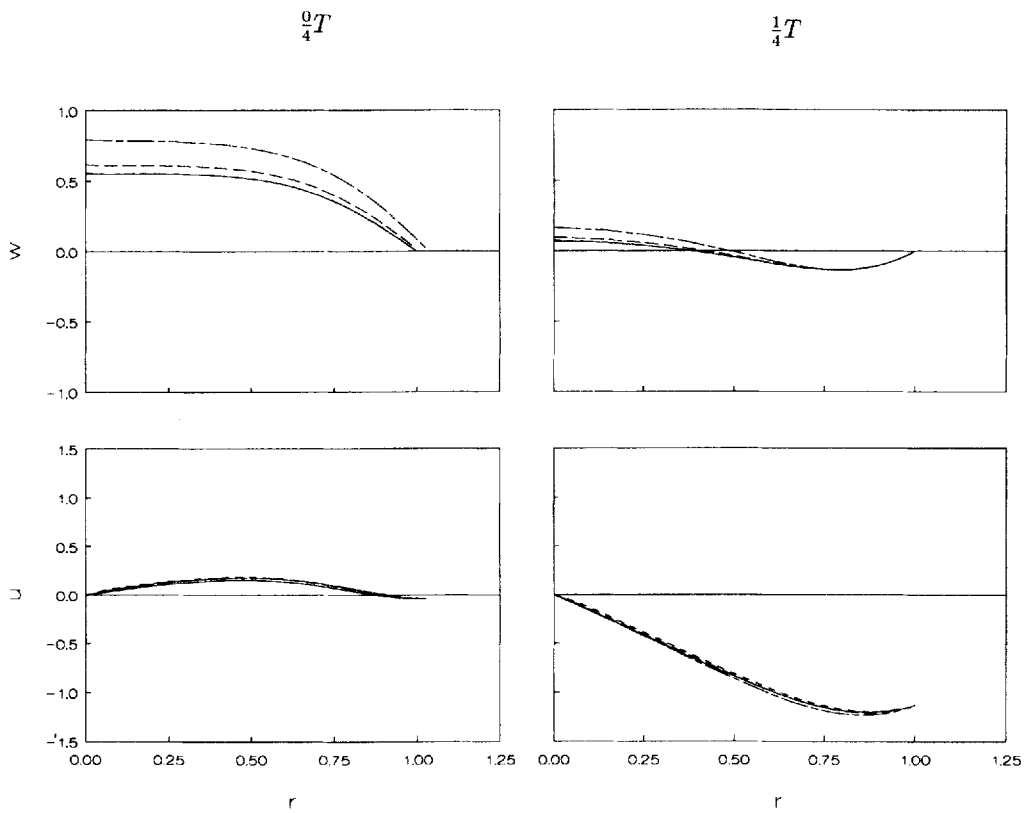

Figure 4. Comparison of the numerically calculated axial and radial velocity profiles, w and u respectively, at $z = 1$, with the analytical results using Womersley's theory. For legend see Figure 3. The results presented correspond to the solutions at $t = 0T$ and $t = T/4$

discrepancies appearing. This can be explained from the fact that only the square of G plays a role in the equations of fluid flow.

All calculations mentioned above were carried out using outflow conditions of type 2 [equations (23) and (24)]. The influence of the type of outflow conditions chosen was studied for the physiologically relevant range by making calculations for $\alpha=5$, $S=0{\cdot}2$ and $G=0{\cdot}0001$. No significant differences, $\mathcal{O}(10^{-4})$, were found between solutions obtained using the comprehensive equations (23) and (24) or the simplified equations (25) and (26) for the prescription of the normal and tangential components of the stress vector at the outflow. Prescription of the radial and axial velocity components at the outflow [type 1: equations (19) and (20)] results in significant differences, partly due to the fact that Womersley's solution is incorrect at large speed ratios. The speed ratio not only quantifies the relative diameter changes [equation (15)] but is also proportional to the contribution of the convective term in the equations for the fluid [equations (16) and (17)]. The assumption of the speed ratio being small allowed Womersley to simplify the equations for the fluid flow by omitting the convective terms. In order to study the contribution of the convective terms to our numerical solution, the solution of the Stokes equation was computed. A speed ratio $S=0{\cdot}2$ was taken. Again $\alpha=5$ and $G=0{\cdot}001$ were taken. Comparison with the corresponding solution of the Navier–Stokes equation revealed differences in the velocities of up to 5 per cent of the maximum velocity.

FLOW IN A DISTENSIBLE TUBE WITH A LOCAL INHOMOGENITY

*Governing equations**

To illustrate the method, fluid flow in a distensible tube containing a section with a different compliance and diameter (Figure 5) was analysed. An overview of the properties of the tube is given in Table II. The time-dependent pressure distribution was calculated using a model for the wave propagation in the tube. This is more complicated than for the uniform tube. The inhomogeneity of the tube might have a marked influence on the wave propagation: a forward-travelling wave (p_f) will be partly transmitted (p_t), and partly reflected (p_b). Recently, we developed and tested a model to calculate the propagation of waves in tubes with a local inhomogeneity with a length much smaller than the relevant wavelengths[8]. Using this model, expressions are found for the reflection and transmission coefficients, relating the forward- and backward-travelling waves at the proximal end of the inhomogeneity and the forward-travelling and transmitted waves at the distal end of the inhomogeneity, respectively. The time-dependent pressure distribution outside the inhomogeneity can be obtained by applying wave propagation theory to the forward, reflected and transmitted waves:

section A_1:

$$\begin{aligned} p(z,t) &= p_f(z,t) + p_b(z,t) \\ &= \mathrm{Re}\left[p_0 e^{2\pi j w(t-z/c)} + p_0 \Gamma e^{2\pi j w(t-(2z_2-z)/c)}\right], \end{aligned} \tag{27}$$

section A_2:

$$\begin{aligned} p(z,t) &= p_t(z,t) \\ &= \mathrm{Re}\left[p_0 e^{2\pi j w(t-z_2/c)} T e^{2\pi j w(z-z_5)/c)}\right], \end{aligned} \tag{28}$$

* For convenience, the equations in this section are not presented in their non-dimensional form, but are expressed in terms of physical quantities.

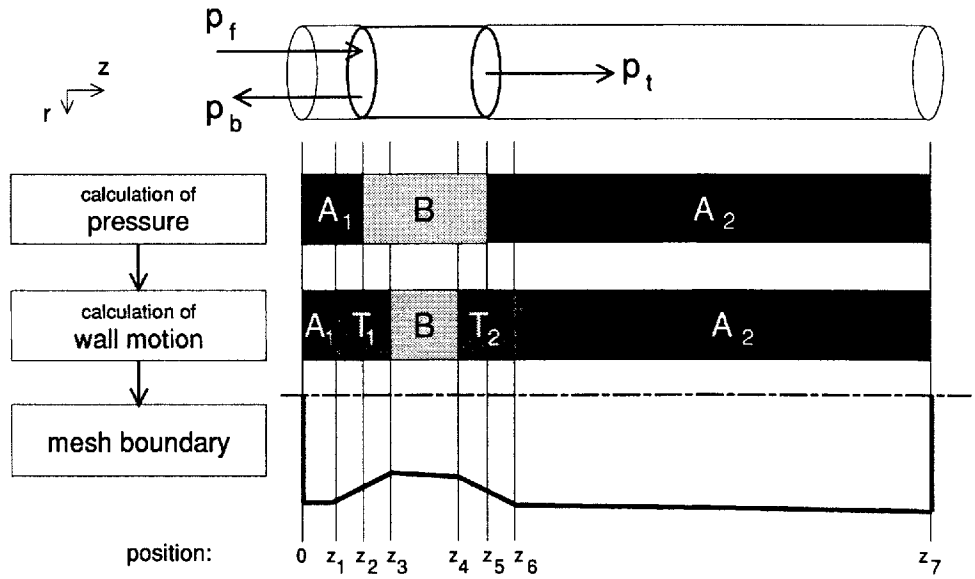

Figure 5. Schematical representation of the solution strategy used for the uniform tube with a local inhomogeneity.

Table II. Properties of the distensible tube with a local inhomogeneity

$z_1 = 0{\cdot}05$	$\alpha_{tube} = 5$	$R_{tube} = 5 \times 10^{-3}$
$z_2 = 0{\cdot}1$	$S_{tube} = 0{\cdot}05$	
$z_3 = 0{\cdot}15$	$G_{tube} = 0{\cdot}001$	$R_{inhom} = 4 \times 10^{-3}$
$z_4 = 0{\cdot}25$		
$z_5 = 0{\cdot}3$	$\Gamma = -0{\cdot}054 + 0{\cdot}094j$	
$z_6 = 0{\cdot}35$	$T = 0{\cdot}74 - 0.48j$	
$z_7 = 1.0$		

with $p_0 = p_f(0, 0)$, Γ the reflection coefficient and T the transmission coefficient. The time-dependent pressure distribution in the inhomogeneity is obtained using linear interpolation between the pressures calculated at the proximal and distal end:

section B:

$$p(z, t) = p(z_2, t) + \frac{z - z_2}{z_5 - z_2} [p(z_5, t) - p(z_2, t)]. \tag{29}$$

It is assumed that no reflected waves arise from the termination. To calculate the wall motion, a numerical model on the basis of geometrically non-linear deformation theory and an appropriate material model has to be developed. For now, the wall motion is calculated in a simplified way from the local pressure and compliance. Again it is assumed that there is only wall motion in the radial direction:

sections A_1, B and A_2:

$$R(z, t) = R_0(z) + \frac{p(z, t) C(z)}{2\pi R_0}. \tag{30}$$

Because this approach would introduce sharp discontinuities in the wall position at the junction between sections A_i and B, transition sections T are introduced for which the wall position is calculated as:

section T_1:

$$R(z, t)=R(z_1, t)+\frac{z-z_1}{z_3-z_1}[R(z_3, t)-R(z_1, t)], \tag{31}$$

section T_2:

$$R(z, t)=R(z_4, t)+\frac{z-z_1}{z_6-z_4}[R(z_6, t)-R(z_4, t)]. \tag{32}$$

The boundary of the element mesh to be generated is described by equations (30)–(32). The length of the tube is chosen to be equal to 0·2 wavelength. As inflow condition ($z=0$), a fully developed velocity profile was prescribed. The velocity profile is again related to the pressure according to

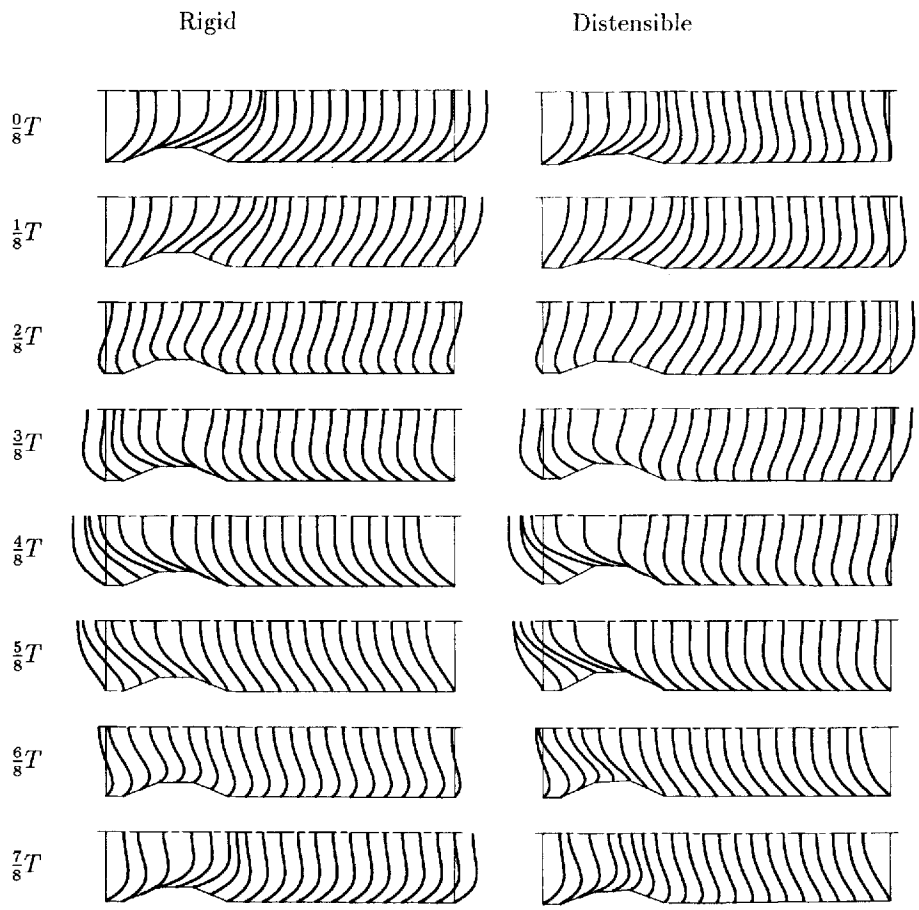

Figure 6. Axial velocity profiles at equidistant timesteps for (a) the rigid and (b) the distensible tube respectively

Womersley's theory:

$$w(y, 0, t) = \mathrm{Re}\left\{\frac{R_0^2}{R^2}[p_f(0, t) - p_b(0, t)]\frac{1}{\rho c}\left[1 - \frac{J_0(\alpha j^{3/2} y)}{J_0(\alpha j^{3/2})}\right]\right\}, \tag{33}$$

$$u(y, 0, t) = \mathrm{Re}\left\{[p_f(0, t) - p_b(0, t)]\frac{j\omega R_0}{2\rho c^2}\left[-\frac{2J_1(\alpha j^{3/2} y)}{\alpha j^{3/2} J_0(\alpha j^{3/2})} + y\right]\right\}. \tag{34}$$

In order to guarantee a sinusoidal flow at the entrance, the term R_0^2/R^2 was added in equation (33), as described in the preceding section. The boundary conditions at the tube axis and the wall are identical to the ones used for the uniform tube [equations (21) and (22)]. Outflow conditions of type 3 were chosen [equations (25) and (26)] in the calculations for the distensible geometry.

For comparison, the flow field in a corresponding rigid geometry was calculated using the same inflow conditions [equations (33) and (34)]. A stress free outflow condition, $\sigma_n = 0$, $\sigma_t = 0$, was applied. The time integration scheme was identical to the one used for the uniform tube. The penalty parameter was chosen equal to $\varepsilon = 10^{-6}$.

Results and discussion

Figures 6(a) and 6(b) show the computed axial-velocity profiles for the rigid and distensible tubes, respectively. A striking difference is, of course, that the outflow profile of the rigid tube is equal to the inflow profile, while the outflow profile of the distensible tube has a different phase. This is a logical consequence of the finite velocity with which disturbances travel through the distensible tube. The diameter of the inhomogeneity in the distensible tube is maximal during positive inflow, and minimal during negative inflow. This results in less acceleration of the fluid compared to the rigid tube during positive inflow, and more acceleration during negative inflow.

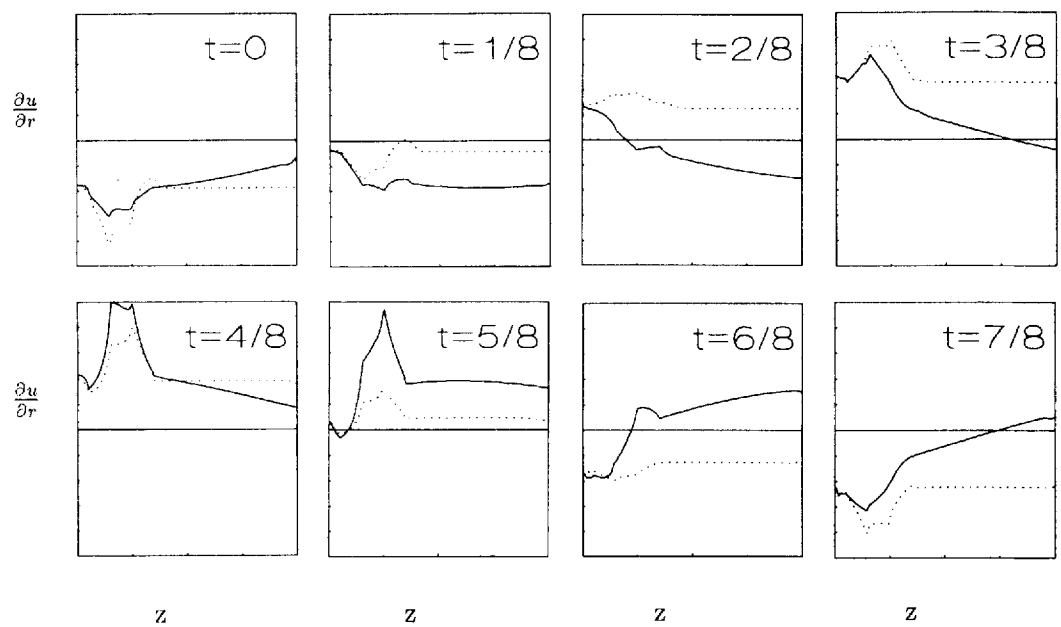

Figure 7. Comparison of the velocity gradients at the wall as a function of axial position calculated for the rigid (· · · · ·) and distensible (——) tube at equidistant timesteps

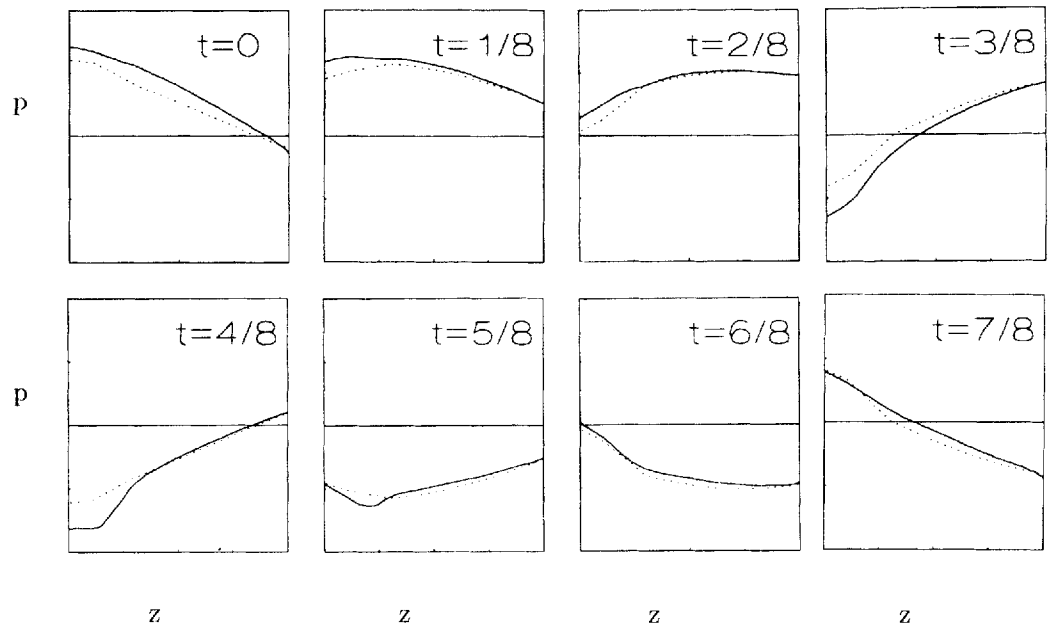

Figure 8. Comparison of the pressure calculated from the numerical solution for the flow field in the distensible tube (——) with the pressure calculated from wave propagation (· · · · ·), both as a function of the axial position and at equidistant timesteps

This has its influence on the wall shear stress too. In Figure 7 the velocity gradients, calculated for the rigid and distensible tube as a function of position, are compared. In the distensible tube the velocity gradients are somewhat less negative during the inflow phase and significantly higher during the negative inflow phase.

Finally, the pressure distribution calculated from the numerical solution of the velocity field is compared with the pressure distribution calculated on the basis of wave propagation [equations (27)–(29)]. If significant discrepancies should show up, the solution obtained using the uncoupled strategy is not consistent. In that case the pressure distribution calculated from the numerical solution of the velocity field gives rise to a wall motion different from the one applied on basis of the calculation of wave propagation. For our test example Figure 8 shows a fair agreement between the pressure distribution given by equations (27)–(29) and the computed pressure on the tube axis. Only at $t=3/8$ and $t=4/8$ discrepancies are found around the inhomogeneity, indicating that the pressure should be somewhat lower, which should enforce the effects of the distensibility. Realizing that major simplifications were made in the calculation of the wall motion, it is probably too early to draw conclusions about the accuracy of our numerical solution. Nevertheless, no indications were found contradicting the applicability of the strategy described.

CONCLUSIONS

A numerical strategy based on the uncoupled solution of wall motion and fluid flow was introduced for the analysis of the flow in distensible geometries. It was estimated that this strategy is applicable if the ratio between fluid and wave velocity, $S=u/c$, is small. The strategy was studied by making calculations of the flow field in a uniform distensible tube and comparing these calculations with an analytical solution valid for $S \ll 1$ and $G \ll 1$. For such small values of the

speed ratio and the ratio between radius and wavelength (in our calculations: $S=0{\cdot}0005$, $G=0{\cdot}0001$), a perfect agreement between numerical and analytic solution was found. The agreement remained fair for values of S up to 0·05, and G up to 0·1. The discrepancies found at higher values of S might have two possible sources. The effect of neglecting the changing cross-sectional area in the derivation of the analytic solution is dominant, the omission of the convective terms is of less importance. The numerical solution found is relatively insensitive to the value of G. Only at values far outside the physiologically relevant range, $G>0{\cdot}1$, discrepancies with the analytic solution are found. As already mentioned, this is probably due to the fact that only G^2 plays a role in the equations of fluid flow. On the same grounds, it is possible to use simplified expressions for the outflow conditions, $\sigma_n=0$, $\sigma_t=0$.

It is impossible to define the range of applicability of our numerical strategy on the basis of comparison with an analytical solution which itself has only limited applicability. An important criterion in estimating the validity of the numerical solution obtained was the comparison of the numerically obtained pressure with the pressure calculated on the basis of wave propagation and was used as input for the calculation of the wall motion. If large discrepancies are found, the numerically obtained solution is not consistent: in that case, the numerically obtained pressure suggests that a different wall motion should have been prescribed. For the uniform tube, with the inflow corrected to be sinusoidal, significant discrepancies begin to show up from values of $S>0{\cdot}1$. The findings in this study indicate that the uncoupled strategy seems to be useful, at least to obtain an insight into the effect of the wall distensibility on the flow phenomena. Convective effects might, however, play a more important role in more complicated distensible geometries than in the uniform tubes studied in this report. In that case, one might consider the use of this strategy in an iterative way: with the pressure distribution calculated from the numerical solution for the flow field, a new wall motion is calculated, which results in new boundary conditions for the solution of the equations of the fluid flow. At this moment, it is not possible to say if such an iterative strategy is stable. Problems similar to the ones occurring when using a 'weakly coupled' strategy[1] occur when an appropriate extrapolation algorithm has to be chosen.

With the analysis of the flow in a uniform tube with a local inhomogeneity, we tried to illustrate the possibilities of our strategy. It was shown that the distensibility of the geometry might have significant influence on the flow phenomena, not only because of the wave phenomena occurring but also because of the wall motion changing the geometry. The need for a numerical model for the calculation of wall motion due to the time-dependent pressure distribution became quite prominent, and will be the next thing to pay attention to in the further development of our strategy.

REFERENCES

1. D. Hilbert, 'An efficient Navier–Stokes solver and its application to fluid flow in elastic tubes', in *Numerical Methods, Colloquia Societatis Janos Bolya*, vol. 50, North–Holland, Amsterdam, 1986, pp. 423–431.
2. P. J. Reuderink, P. J. B. Willems, P. J. G. Schreurs and A. A. van Steenhoven, 'Fluid flow through distensible models of the carotid artery bifurcation', in D. Liepsch (ed.), *Biofluid Mechanics, Blood Flow in Large Vessels*, Springer, Berlin, 1989, pp. 329–334.
3. J. Lighthill, *Waves in Fluids*, Cambridge University Press, Cambridge, 1978.
4. W. R. Milnor, *Hemodynamics*, Williams and Wilkins, Baltimore, 1982.
5. J. R. Womersley, The mathematical analysis of the arterial circulation in a state of oscillatory motion', Wright Air Development Center, *Tech. Report WADC–TR56–614*, 1957.
6. J. B. A. M. Horsten, A. A. van Steenhoven and M. E. H. van Dongen, 'Linear propagation of pulsatile waves in visco-elastic tubes', *J. Biomechanics*, **22**, 477–484 (1989).
7. P. J. Reuderink, H. W. Hoogstraten, P. Sipkema and N. Westerhof, 'Linear and non-linear one-dimensional models of pulse wave propagation at high Womersley numbers', *J. Biomechanics*, **22**, 819–827 (1989).
8. P. J. Reuderink, H. J. De Heus, M. E. H. van Dongen and A. A. van Steenhoven, 'A model for wave reflection at the carotid artery bifurcation', (submitted to *J. Biomechanics*)

9. C. Cuvelier, A. Segal and A. A. van Steenhoven, *Finite Element Methods and Navier–Stokes Equations*, Reidel, Dordrecht, The Netherlands, 1986.
10. A. Segal, *SEPRAN User Manual, Standard Problems and Programmers Guide*, Ingenieursbureau SEPRA, Leidschendam, The Netherlands, 1984.
11. F. N. van de Vosse, A. A. van Steenhoven, A. Segal and J. D. Janssen, 'A finite element analysis of the steady laminar entrance flow in a 90° curved tube', *Int. j. numer. methods fluids*, **9**, 275–287 (1989).
12. F. N. van de Vosse, 'Numerical analysis of carotid artery flow', *Ph.D. Thesis*, Eindhoven University of Technology, The Netherlands, 1987.
13. F. N. van de Vosse, A. Segal, A. A. van Steenhoven and J. D. Janssen, 'A finite element approximation of the unsteady two-dimensional Navier–Stokes equations', *Int. j. numer. methods fluids*, **6**, 427–443 (1986).